

DETACHED EDDY SIMULATION OF HYPERSONIC SHOCK-WAVE/BOUNDARY-LAYER INTERACTIONS ON HIFIRE-1 AXISYMMETRIC CONE-CYLINDER-FLARE

Romie Oktovianus Bura^{1,2}, Ahmad Riyadl³

¹Faculty of Defense Science and Technology, Republic of Indonesia Defense University (RIDU), Bogor 16810, Indonesia

²Faculty of Mechanical and Aerospace Engineering, Bandung Institute of Technology (ITB), Bandung 40132, Indonesia

³Research Organization for Aeronautics and Space, National Research and Innovation Agency (BRIN), Cibinong 16911, Indonesia

Abstract

In the present work, the turbulent Shock-Wave/Boundary-Layer Interactions (SWBLIs) over a geometry model of HIFiRE-1 Axisymmetric Cone-Cylinder-Flare with a ramp angle of 33° at Mach 7.16 were analyzed, using Detached Eddy Simulation (DES) and $k-\omega$ turbulence models. Structured hexahedral meshing was used to perform the computation domain and the simulations presented critical characteristics in SWBLIs, such as wall pressure distribution, wall shear stress distribution and wall heat flux. The simulation results were compared to the experimental result of HIFiRE-1 ground test studies.

Keywords: DES, Hypersonic, SWBLIs, HIFiRE-1, Turbulent

1. Introduction

Shock-Wave/Boundary-Layer Interactions (SWBLIs) are among the many issues in maintained flight at hypersonic speeds that present challenges to aerospace vehicle design and still poorly understood [1]. At hypersonic speed, the aerothermal conditions are very extreme, which can impact the surface pressure load and heating of a vehicle and cause heating which generates on the body such as on the leading edge of the wing which is responsible for system failure [2,3]. The shock-dominated flows typical of hypersonic flight can show interference effects that increments surface heat transfer rates extraordinarily [4,5]. Thus, the design configuration of such a vehicle should be under acceptable consideration.

SWBLIs also may lead to boundary layer separation, enhancing heating load, or even turbulent reattachment. A typical schematic diagram for ramp-induced SWBLIs is shown in Figure 1. In the presence of the ramp the flow becomes deflected abruptly by the compression corner with its associated adverse pressure gradient, which leads to the generation of oblique shock waves emanating from the compression corner that interacts with the boundary layer over the wall. Hence, the boundary layer experiences an adverse pressure gradient near the region of the flow deceleration. If the deflection angle is higher than the incipient separation angle, the boundary layer separation takes place well ahead of the compression corner and separation shock forms ahead of the separation region due to the coalescence of compression waves induced by the separation process.

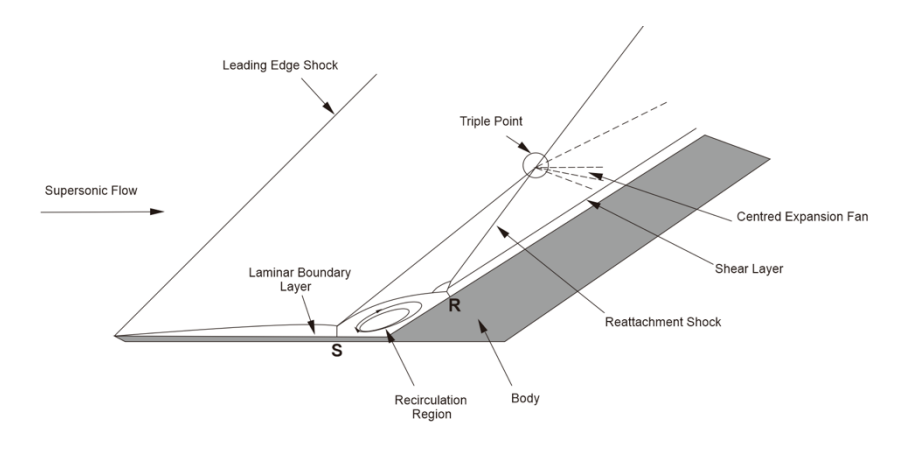


Figure 1 - SWBLIs in compression ramp

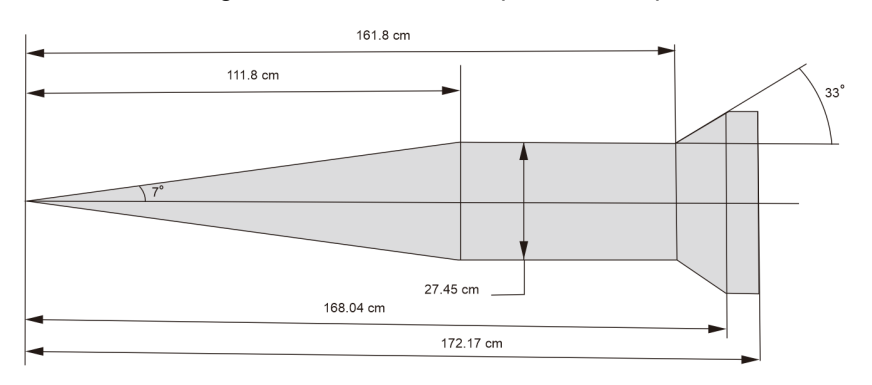


Figure 2 - HIFiRE-1 model dimension

The nearly constant plateau pressure region downstream of the separation point is invariantly considered as the indicator to identify the separation bubble. This recirculation zone extends up to the reattachment point, where the flow re-attaches on the ramp surface [6]. The peak heat-flux rate near the reattachment point (or boundary layer neck) may be much larger than that of elsewhere. In general, the peak heating on a compression ramp may be determined by the state of the separated flow as it re-attaches to the ramp surface [7, 8]. However, the detail of this process may vary depending on the case and if it is examined in a different state [9].

The modeling of turbulent SWBLIs is one of the keys to predicting the pressure and heating load, which impacts on vehicle body [10]. The state-of-the-art turbulence simulations in engineering applications are mainly solving the Reynolds-Averaged Navier-Stokes (RANS) equations. The associated turbulence modeling remains a major source of uncertainty in the computational prediction of aerodynamic forces and heating for hypersonic vehicles. Currently, the most accurate computational modeling is by the Direct Numerical Simulation (DNS) and the challenge is the number of grid cells. Hence, for a high Reynolds number simulation, the level of computation requirement will be extremely high. The Large Eddy Simulation (LES), while requiring relatively much less than DNS, still requires significant amount of computation. The intermediate model is Detached Eddy Simulation (DES). In this model, RANS formulation is used for the near wall regions and LES is used for the free stream.

In the present study the pressure and heating load on the HIFiRE-1 vehicle, with a ramp angle of 33° at Mach 7.16 inducing strong turbulent SWBLIs, as well as other important phenomena such as point of separation and reattachment from DES and $k-\omega$ turbulence modelling were compared with experimental data published [11-13]. The ground test of HIFiRE-1 experiments has been developed in the LENS-1 to study the full-scale flight vehicle at selected conditions along the test flight trajectory, which in the future can be used to design the next-generation hypersonic vehicle [14]. The schematic diagram of the HIFiRE-1 body is shown in Figure 2.

While HIFiRE-1 configuration is Axisymmetric Cone-Cylinder-Flare, its flow physics is similar to compression ramp without the issue of three-dimensionality. Some related works correspondence in hypersonic flows over a ramp are the study of the surface pressure and heat flux in hypersonic laminar interactions with real gas effects by Hao et al. [15], the effect of leading-edge bluntness toward separation bubble size, boundary layer edge Mach number and temperature, sonic height, boundary layer thickness, skin friction coefficient and pressure by John et al. [16], the studies of unsteady behavior of interaction from hypersonic and air with its thermochemical non-equilibrium effects [17-20], the study of shock wave unsteadiness in SWBLIs over compression ramp by Sun et al. [21], 3D (Three Dimensional) model simulation for compression ramp studied by Oliver et al. [22] and 3D cone with a control surface studied by Pandey et al. [23], the experimental study of coneflare with different blunt radius and flare angle as well as Reynolds number by Running et al. [24]

The present studies are a part of fundamental research of SWBLIs in hypersonic flows for better experimental and numerical integration by using existing experimental results as the basis for numerical predictions, in this case is the turbulence modelling of DES, with the aim to develop strategies for efficient numerical methods in hypersonic vehicle design. The present studies also aim to compare several turbulence models with experimental results of HIFiRE-1 and based on our knowledge, the study DES for the turbulent SWBLI study in the HIFiRE-1 vehicle model has never been performed. For that purpose, the result of $k-\omega$ turbulence model is also presented. The present work is the continuation of the work presented at 33rd ICAS 2022, in Sweden [25].

2. Methods

The 3D model of fluid domain around the HIFiRE-1 body was modeled as a 2D (Two Dimensional) structured hexahedral mesh. The 2D quad mesh was then computed as axisymmetric in the solver to mimic the flow in a real 3D model. The computational domain taken in this simulation is the upper portion above the HIFiRE-1 surface. Figure 3 shows the fluid domain and its boundary condition assigned on each side of the domain, ensuring that all-important physics flows could be captured and the refinement was given on the wall surface and the junction between leading-edge, conecylinder, cylinder-flare, and flare-aft. To catch important physical flow near the wall, the value of y+was adjusted close to 1. The mesh element size for each blocking was also adjusted by creating bunching along the edges, which separated among the blocks as such that the relative mesh size in the edge of each block was close to the mesh size in the neighboring block.

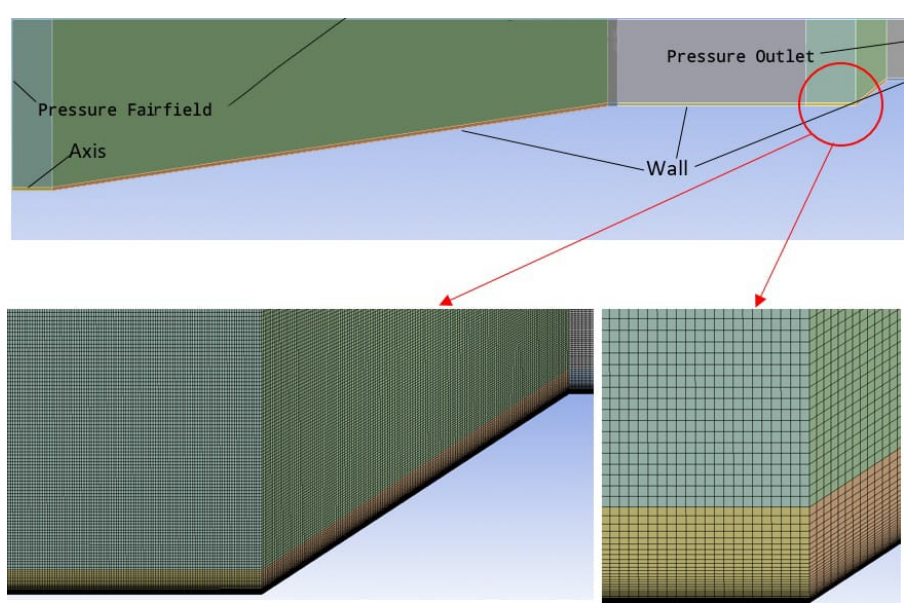


Figure 3 - Boundary condition on fluid domain and meshing

The inlet and far-field were assigned as pressure-inlet, the outlet was assigned as pressure-outlet, the wall assigned with no-slip wall and isothermal with determined temperature, and the symmetry as an axis. The assigned boundary condition of the inlet, outlet, wall, far-field, and symmetry have input values as in Table 1 below.

Table 1. Boundary Condition Values

| | Inlet | Outlet | Wall | Farfield | Axis |
|-----------------|-------|--------|------|----------|------|
| Pressure (Pa) | 4620 | 4620 | - | 4620 | - |
| Mach Number | 7.16 | - | - | 7.16 | - |
| Temperature (K) | 231.7 | 231.7 | 299 | 231.7 | - |

For $k-\omega$ turbulence model, the solver was set up to the density-based setting due to the concern of the air compressibility effect in hypersonic flows [10]. The fluid is assumed to be an ideal gas for present studies, the coefficient of dynamic viscosity (μ) is calculated by making use of Sutherland's law [26]. The solution methods formulation was chosen to be implicit with the flux type Roe-FDS. The spatial discretization gradient was chosen to Green-Gauss Node Element and the modified turbulent viscosity to be first-order upwind and the transient formulation to be second-order implicit. The simulation conducted using transient analysis as the main flow features, such as the entire laminar separated region, the strong bow-shock, the triple point and the location of the separation shock show an unsteady [27] and time-dependent behaviour [28]. The study about computational test time on double compression hypersonic flow with averaged data from timestep by Durna et al. [29] and another experimental study by Swantek et al. [30]. The equations for $k-\omega$ turbulence modeling in this present work are below (1) and (2) based on the references [31,32]:

$$\frac{\partial}{\partial t}(\rho k) + \frac{\partial}{\partial x_i}(\rho k u_i) = \frac{\partial}{\partial x_j} \left(\Gamma_k \frac{\partial k}{\partial x_j} \right) + G_k - Y_k + S_k \tag{1}$$

$$\frac{\partial}{\partial t}(\rho\omega) + \frac{\partial}{\partial x_i}(\rho\omega u_i) = \frac{\partial}{\partial x_j}\left(\Gamma_\omega \frac{\partial\omega}{\partial x_j}\right) + G_\omega - Y_\omega + S_\omega \tag{2}$$

Where k is the turbulence kinetic energy, ω is the specific dissipation rate, G_k is the generation of turbulence kinetic energy due to mean velocity gradients, G_ω is the generation of ω , while Y_k and Y_ω are the dissipation of k and ω due to turbulence. Γ_k and Γ_ω are the effective diffusivity of k and ω , respectively, while S_k and S_ω are user-defined source terms.

Detached Eddy Simulation (DES) was introduced by Spalart and co-workers to eliminate the main limitation of LES models. DES uses RANS model for the attached boundary layer and LES for the separated flow. The advantage of this model is its cost, less expensive than LES especially for high Reynolds number, and its accuracy compare to RANS, for unsteady and 3D flow [33]. By this formulation, the wall boundary layers are entirely covered by the RANS model and the free shear flows away from walls are typically computed in LES mode. Based on the references [33-35], the transport equation of Spalart-Allmaras model is below (3):

$$\frac{\partial \tilde{v}}{\partial t} + \tilde{u}_j \frac{\partial \tilde{v}}{\partial x_j} = \tilde{S} \tilde{v} c_{b1} + \frac{1}{\sigma} \frac{\partial}{\partial x_j} \left((v + \tilde{v}) \frac{\partial \tilde{v}}{\partial x_j} \right) + \frac{c_{b2}}{\sigma} \left(\frac{\partial \tilde{v}}{\partial x_j} \frac{\partial \tilde{v}}{\partial x_j} \right) - c_{w1} f_w \left(\frac{\tilde{v}}{d} \right)^2$$
(3)

The transported variable in the Spalart-Allmaras model, \tilde{v} , is identical to the turbulent kinematic viscosity except in the near-wall (viscosity-affected) region. The variables cb1, cb2, and σ are constants. The turbulent viscosity, μ_t , is computed from equation (4), where the viscous damping function, f_{v1} , is given by equation (5):

$$\mu_t = \bar{\rho}\tilde{v}f_{v1} \tag{4}$$

$$f_{v1} = \frac{X^3}{X^3 + c_{v1}^3}$$
 , $X = \frac{\tilde{v}}{v}$ (5)

and equation (6):

$$\tilde{S} = S + \frac{v}{\kappa^2 d^2} \tag{6}$$

where κ is constant and S is a scalar measure of the deformation tensor. The value S is based on the magnitude of the vorticity.

The DES approach used is based on the Spalart-Allmaras turbulence model in equations (3) and (4). To obtain the model used in the DES formulation, the length scale (*d*) of the S-A destruction term is modified in equations (7) and (8) to be the minimum of the distance to the closest wall and a length scale proportional to the local grid spacing,

$$\tilde{d} = \min\left(d, C_{DES}\Delta\right) \tag{7}$$

$$\Delta = \max\left(\Delta x, \Delta y, \Delta z\right) \tag{8}$$

where \tilde{d} is the modified length scale, Δ is the maximum local grid spacing, and C_{DES} is a constant.

3. Result and Discussion

The results of DES and $k-\omega$ turbulence modelling are presented. Table 2 shows the mesh and the result of steady state. It also shows the results of Separation and Reattachment points, x_s and x_r , as well as the Separation Length, x_{bsl} .

Table 2. Mesh and Steady State Condition Result

| i dioio =: inioon dina ottoday ottoday | | | | | | | | | |
|--|---------------------|-------------|--------|-----------|-----------|---------------|--|--|--|
| Turbulence Model | Cell Size | Cell Number | t (ms) | x_s (m) | x_r (m) | x_{bsl} (m) | | | |
| $k-\omega$ | 0.5 mm ² | 131000 | 20 | 1.56 | 1.65 | 0.09 | | | |
| DES | 0.5 mm ² | 131000 | 20 | 1.49 | 1.68 | 0.19 | | | |

The wall shear stress on the body surface in Figure 4 was plotted in the same manner as the wall pressure distribution plot, except that the experimental value taken was only the point of separation as the main concern. The result shows that there is an indication of secondary separation existence from DES result. Secondary separation has been found to exist in previous work of massively-separated turbulent SWBLIs cases. This should warrant further fundamental study to investigate geometrical and flow conditions, as well as its impact, that induce such phenomenon in SWBLIs. However, as shown later by the wall heat flux and wall pressure results, DES simulations turned out to take significantly more time than RANS. Hence, the present work provides both DES approach simulations based on the Spalart-Allmaras and $k-\omega$ turbulence models, shown by the wall heat flux and wall pressure results, for comparison.

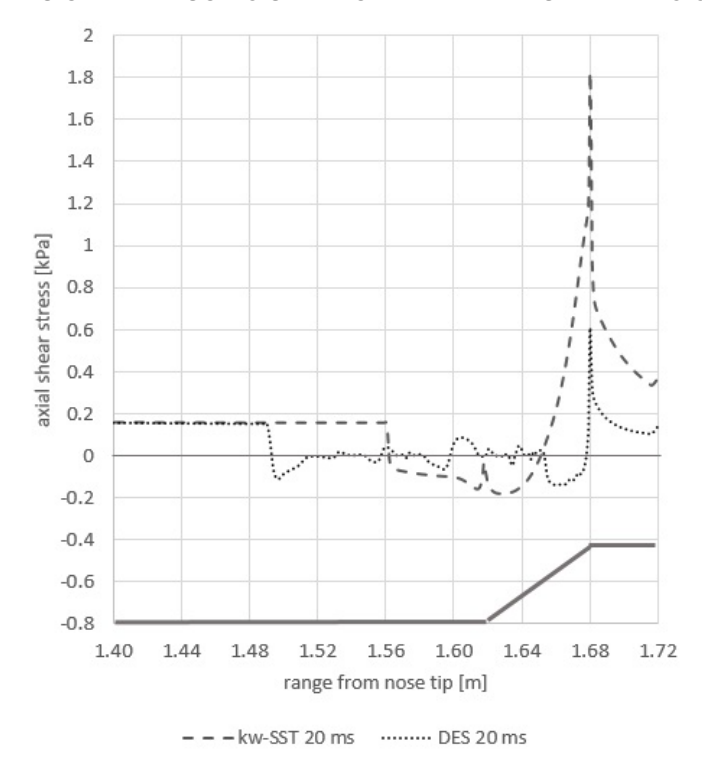


Figure 4 - Wall Shear Stress comparison with experimental results of HIFiRE-1

The results of the wall heat flux for DES based on both Spalart-Allmaras and $k-\omega$ turbulence models are shown in Figure 5 and compared with the experimental results of HIFiRE-1.

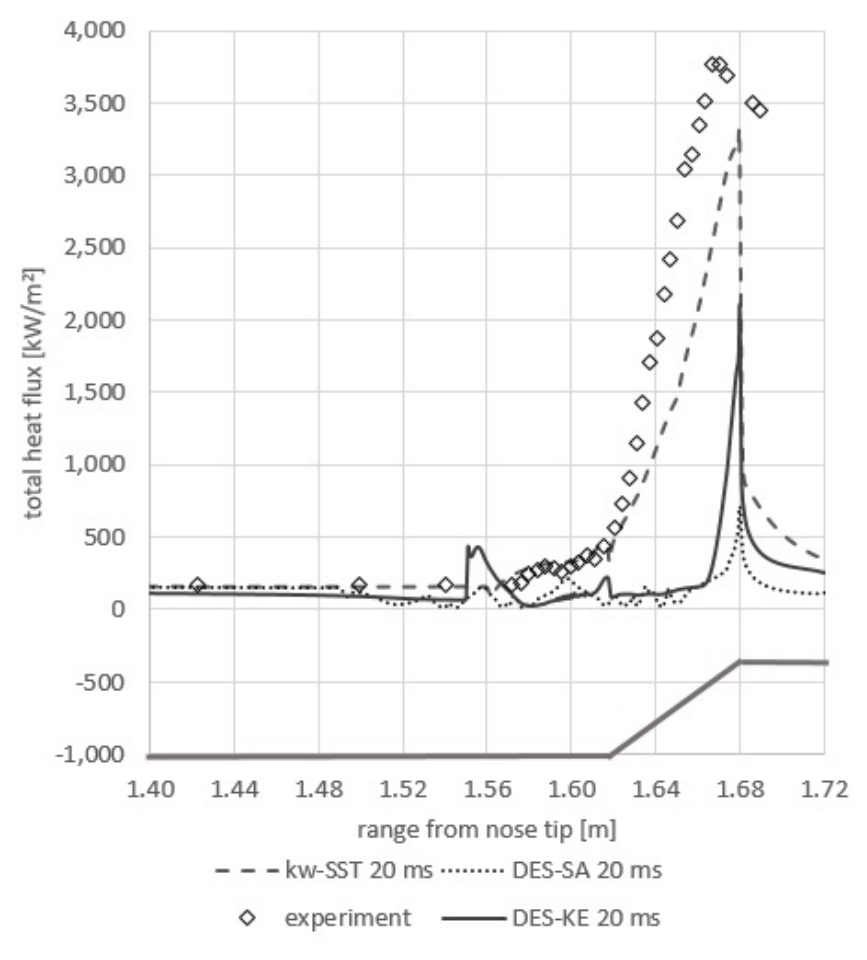


Figure 5 - Wall Heat Flux comparison with experimental results of HIFiRE-1

In the present study, the point of interest is the wall heat flux near the compression ramp (cylinder-flare) region as shown in Figure 5. The result shows that there is a good agreement between $k-\omega$ turbulence modelling and experimental data, even though the $k-\omega$ turbulence modelling underpredicts the peak value of experimental data. However, unlike the $k-\omega$ turbulence modelling, the DES results, based on both Spalart-Allmaras and $k-\omega$ turbulence models, largely underpredicts the experimental data. Based on available data, the computation of DES needs to continue in order to achieve the convergence or steady-state condition.

The comparison for pressure the wall surface is shown in Figure 6, and also compared with the experimental results. For wall pressure the result shows that, similar to the wall heat flux results, there is a good agreement between $k-\omega$ turbulence modelling and experimental data, with underprediction of peak value. And also similarly, the $k-\omega$ - based DES results largely underpredicts the experimental data. And interestingly, the Spalart – Allmaras - based DES shown overpredicts the experimental result. This DES-based simulations of massively-separated turbulent SWBLIs have shown to be a challenging case of complex flow predictions.

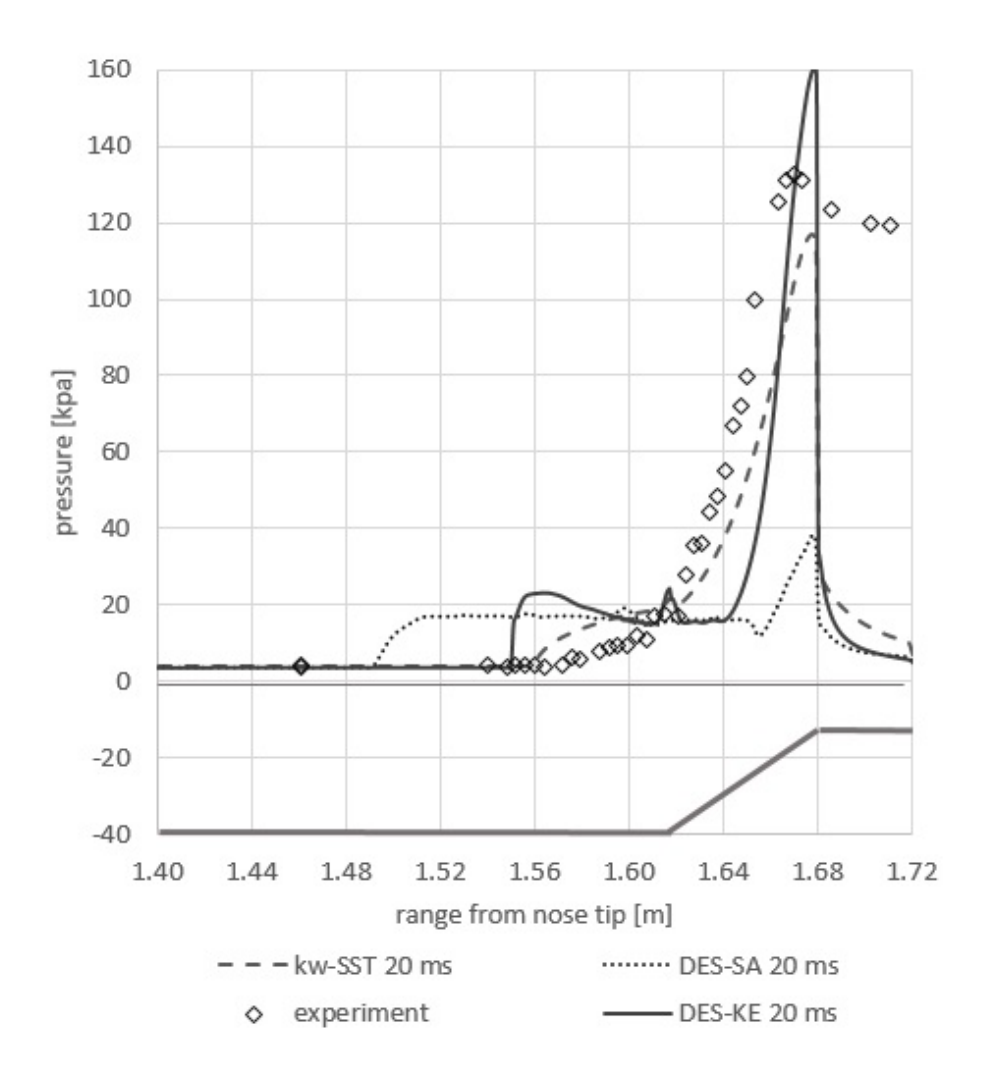


Figure 6 - Wall Pressure comparison with experimental results of HIFiRE-1



Figure 7 – Density gradient contour for $k-\omega$ turbulence model

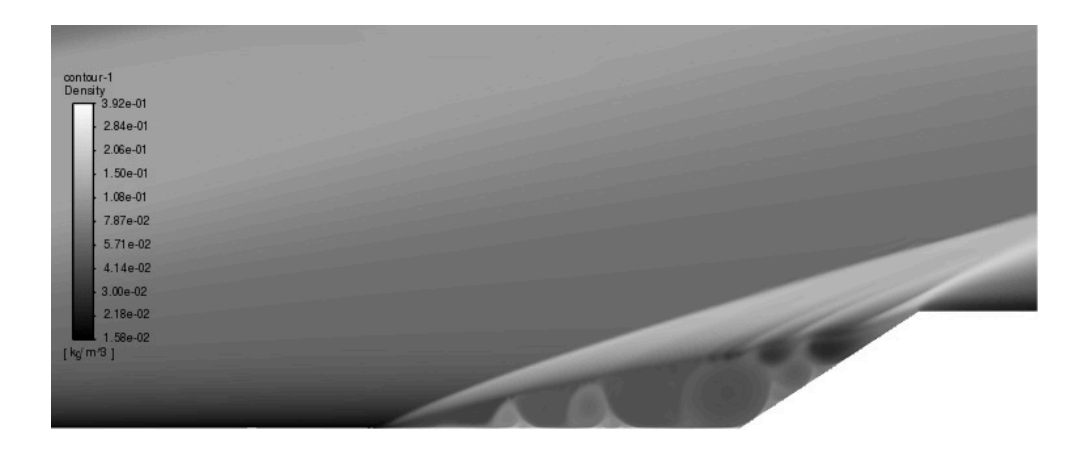


Figure 8 – Density gradient contour for DES turbulence model

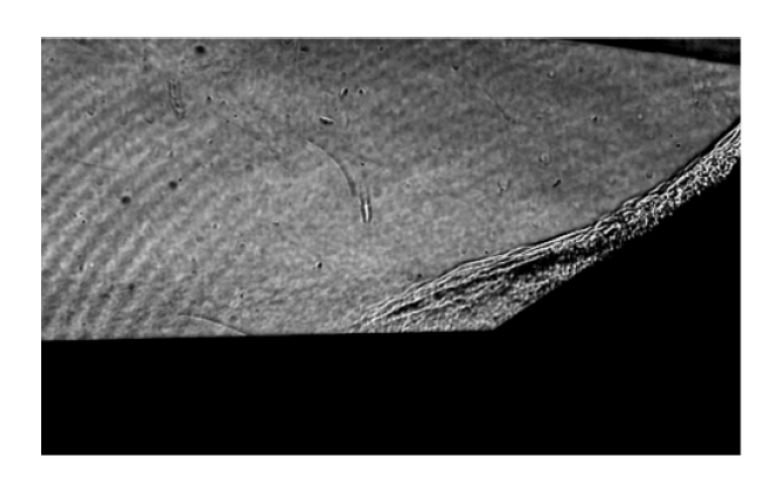


Figure 9 – Schlieren photograph of HIFiRE-1 (with 2.5 mm nose radius)

For the purpose of qualitative study, the Figures 7, 8 and 9 shows the density gradient of $k-\omega$ turbulence and DES modelling. These figures show the flow structure in the region of SWBLIs, and can be compared with the experimental results from Schlieren photograph of HIFiRE-1 (with 2.5 mm nose radius). Similar to experimental results, the DES modelling reveals more complex and detailed structures with possible separation wakes. This is in contrast with RANS-based $k-\omega$ turbulence model, which shows much more simple structure. However, as the quantitative results show, there is a pressing need to continue the DES computing time for more valid results, using both Spalart-Allmaras and $k-\omega$ turbulence models.

4. Conclusion

In the present study of hypersonic flow around HIFiRE-1 body axisymmetric cone cylinder flare with a ramp angle of 33° at Mach 7.16, the steady-state condition of turbulent SWBLIs simulation by DES and $k-\omega$ turbulence modelling have been performed. These results have also been analyzed to compare their accuracy with HIFiRE-1 experimental results. The comparisons show different results of DES and $k-\omega$ turbulence modelling, with respect to experimental results. These comparisons with experimental results justify further studies of DES using both Spalart-Allmaras and $k-\omega$ turbulence models, as $k-\omega$ turbulence modelling provides better result quantitatively. The qualitative results of density gradient, however, reveal better results in terms of more detailed flow structures of DES turbulence modelling compared with $k-\omega$ turbulence modelling. These results show potential of both DES and $k-\omega$ turbulence modelling, which are expected to reveal the numerical and physical aspects of the predictions of massively-separated turbulent SWBLIs cases with aim to develop strategies for efficient numerical methods in hypersonic vehicle design.

5. Data Availability

The data used to support the findings of this study are available from the corresponding author upon request.

6. Conflict of Interest

The author(s) declare(s) that there is no conflict of interest regarding the publication of this paper.

7. Contact Author Email Address

Correspondence should be addressed to Romie Oktovianus Bura, mailto: romiebura@idu.ac.id, romiebura@ae.itb.ac.id and sbli1@yahoo.com

8. Copyright Statement

The authors confirm that they, and/or their company or organization, hold copyright on all of the original material included in this paper. The authors also confirm that they have obtained permission, from the copyright holder of any third-party material included in this paper, to publish it as part of their paper. The authors confirm that they give permission or have obtained permission from the copyright holder of this paper, for the publication and distribution of this paper as part of the ICAS proceedings or as individual off-prints from the proceedings.

9. Acknowledgement

This conference paper and its research process would not have been materialized without support from Indonesia National Research and Innovation Agency (BRIN) for research support, Italian Association of Aeronautics and Astronautics (AIDAA) for scholarship and from our sponsor, **PT Ceria Nugraha Indotama (CNI), Indonesia**. Our gratitude to the management of **PT. CNI Indonesia** for providing generous research as well as travel funding. The authors bear the responsibility for any issues arising from this paper content and publication.

References

- [1] Yentsch R J and Gaitonde D V. Numerical investigation of hypersonic phenomena encountered in HIFiRE flight 1. 50th AIAA Aerosp. Sci. Meet. Incl. New Horizons Forum Aerosp. Expo., January, pp. 1–12, 2012.
- [2] PASHA A A and JUHANY K A. Numerical simulation of compression corner flows at Mach number 9. *Chinese J. Aeronaut.*, vol. 33, no. 6, pp. 1611–1624, 2020.
- [3] Holden M, Wadhams T, MacLean M, Mundy E. Experimental Studies of Shock Wave/Turbulent Boundary Layer Interaction in High Reynolds Number Supersonic and Hypersonic Flows to Evaluate the Performance of CFD Codes. Conference: 40th Fluid Dynamics Conference and Exhibit, pp. 1–23, 2010.
- [4] Badr M A and Knight D D. Shock Wave Laminar Boundary Layer Interaction over a Double Wedge in a high mach Number Flow. *52nd Aerosp. Sci. Meet.*, pp. 1–11, 2014.
- [5] Sullivan B T, Whalen T, Laurence S, and Bodony D J. Direct simulation of fluid-structure interaction in compression ramp with embedded compliant panel. *AIAA Aviat. 2019 Forum*, June, pp. 1–45, 2019.
- [6] John B, Kulkarni V N, and Natarajan G. Shock wave boundary layer interactions in hypersonic flows. *Int. J. Heat Mass Transf.*, vol. 70, pp. 81–90, 2014.
- [7] Tu G, Deng X, and Mao M. Assessment of two turbulence models and some compressibility corrections for hypersonic compression corners by high-order difference schemes. *Chinese J. Aeronaut.*, vol. 25, no. 1, pp. 25–32, 2012.
- [8] Kshitij A, Prince S A, Stollery J L and Ricón F D L P. A simple method for drag estimation for wedge-like fairings in hypersonic flow. *Aeronaut. J.*, vol. 125, no. 1288, pp. 968–987, 2021.
- [9] Hao J, Wen C Y, and Wang J. Numerical investigation of hypervelocity shock-wave/boundary-layer interactions over a double-wedge configuration. *Int. J. Heat Mass Transf.*, vol. 138, pp. 277–292, 2019.
- [10] Aliaga C, Guan K, Selvanayagam Stokes J J, Viti V, and Menter F. Hypersonic applications of the lamina rturbulent transition SST model in ANSYS fluent. *AIAA Aviat. 2020 Forum*, vol. 1, pp. 1–16, 2020.
- [11] MacLean M, Wadhams T P, Holden M, and Johnson H. Ground test studies of the HIFiRE-1 transition experiment Part 2: Computational analysis. *J. Spacecr. Rockets*, vol. 45, no. 6, pp. 1149–1164, 2008.
- [12] Wadhams T P, Mundy E, MacLean M, and Holden M. Ground test studies of the HIFiRE-1 transition experiment part 1: Experimental results. *J. Spacecr. Rockets*, vol. 45, no. 6, pp. 1134–1148, 2008.
- [13] Marvin J G, Brown J L, and Gnoffo P A. Experimental Database with Baseline CFD Solutions: 2-D and Axisymmetric Hypersonic Shock-Wave/Turbulent-Boundary-Layer Interactions. *Nasa/Tm*–2013–216604, no. November, pp. 1–123, 2013.
- [14] MacLean M, Wadhams T P, Holden M and Johnson H. A Computational Analysis of Ground Test Studies of the HIFiRE-1 Transition Experiment. January, pp. 1–20, 2008.
- [15] J. Hao, J. Wang, and C. Lee, "Numerical simulation of high-enthalpy hollow-cylinder/flare flows," *AIAA J.*, vol. 56, no. 8, pp. 3337–3341, 2018.
- [16] John B and Kulkarni V. Effect of leading edge bluntness on the interaction of ramp induced shock wave with laminar boundary layer at hypersonic speed. *Comput. Fluids*, vol. 96, pp. 177–190, 2014.
- [17] Ninni D, Bonelli F, Colonna G, and Pascazio G. Unsteady behavior and thermochemical non equilibrium effects in hypersonic double-wedge flows. *Acta Astronaut.*, vol. 191, no. June 2021, pp. 178–192, 2022.
- [18] Youssefi M R and Knight D D. Assessment of CFD capability for hypersonic shock wave laminar boundary layer interactions. *Aerospace*, vol. 4, no. 2, 2017.
- [19] Knight D *et al.* Assessment of CFD capability for prediction of hypersonic shock interactions. *Prog. Aerosp. Sci.*, vol. 48–49, pp. 8–26, 2012.
- [20] Tchuen G, Burtschell Y, and Zeitoun D E. Numerical study of the interaction of type IV around a double-wedge in hypersonic flow. *Comput. Fluids*, vol. 50, no. 1, pp. 147–154, 2011.
- [21] Sun Z, Gan T, and Wu Y. Shock-wave/boundary-layer interactions at compression ramps studied by high-speed schlieren. *AIAA J.*, vol. 58, no. 4, pp. 1681–1688, 2020.
- [22] Oliver A B, Lillard R P, Blaisdell G A, and Lyrintzis A S. Effects of three-dimensionality in turbulent compression ramp shock-boundary layer interaction computations. *46th AIAA Aerosp. Sci. Meet. Exhib.*, January, 2008.
- [23] Pandey A, Casper K M, Spillers R, Soehnel M, and Spitzer S. Hypersonic shock wave–boundary-layer interaction on the control surface of a slender cone. *AIAA Scitech 2020 Forum*, vol. 1, January, 2020.
- [24] Running C L, Juliano T J, Jewell J S, Borg M P, and Kimmel R L. Hypersonic shock-wave/boundary-layer interactions on a cone/flare. *Exp. Therm. Fluid Sci.*, vol. 109, no. September, p. 109911, 2019.
- [25] Bura R O, Maulana F A. Turbulence Modelling Studies of Shock-Wave/Boundary-Layer Interactions on Hifire-1 Axisymmetric Cone Cylinder Flare in Hypersonic Flows. 33th ICAS Congress, 2022.
- [26] Sutherland W, "LII. The viscosity of gases and molecular force. *London, Edinburgh, Dublin Philos. Mag. J. Sci.*, vol. 36, no. 223, pp. 507–531, 1893.

- [27] Verma S B and Koppenwallner G. Unsteady Separation in Flare-Induced Hypersonic Shock-Wave Boundary-Layer Interaction Flowfield. Vol. 39, no. 3, pp. 467–470, 2002.
- [28] Tumuklu O, Levin D A, and Theofilis V. Effects of Reynolds Number on Laminar Boundary Layer Shock-Interaction Hypersonic Flows on a Double Cone. 2018 Fluid Dyn. Conf., pp. 1–21, 2018.
- [29] Durna A S, Ali Barada M E H, and Celik B. Shock Interaction Mechanisms on a Double Wedge at Mach 7. *Phys. Fluids*, vol. 28, no. 9, 2016.
- [30] Swantek A B and Austin J M. Heat Transfer on a Double Wedge Geometry in Hypervelocity Air and Nitrogen Flows. 50th AIAA Aerosp. Sci. Meet. Incl. New Horizons Forum Aerosp. Expo., pp. 1–12, 2012.
- [31] Canonsburg T D. ANSYS Fluent Theory Guide. *ANSYS Inc.*, *USA*, vol. 15317, no. November, p. 814, 2013, [Online]. Available: http://www.afs.enea.it/project/neptunius/docs/fluent/html/th/main_pre.htm.
- [32] Zhang C, Xu J, Gao L, and Gao G. Studies of compression corner flowfields using three turbulent models," *Procedia Eng.*, vol. 31, pp. 762–768, 2012.
- [33] Huck V, Morency F, Beaugendre H. Grid study for Delayed Detached Eddy Simulation's Grid of a Pre-Stalled Wing. CASI Aero 2019 Canadian Aeronautics and Space Institute's AERO 2019 Conference, May 2019.
- [34] Kostic C. Review of the Spalart-Allmaras Turbulence Model and its Modifications to Three-Dimensional Supersonic Configurations. Scientific Technical Review, Vol.65, No.1, pp.43-49, 2015.
- [35] Yang L, Yue L, Zhang Q, Zhang X. High-order Simulation Solving Navier-Stokes Equations with Spalart–Allmaras Turbulence Model. Journal of Physics: Conference Series, 1600, 2020.